



Full Text View

[Volume 28, Issue 6 \(June 1998\)](#)

Journal of Physical Oceanography

Article: pp. 1071–1088 | [Abstract](#) | [PDF \(426K\)](#)

An OGCM Study for the TOGA Decade. Part I: Role of Salinity in the Physics of the Western Pacific Fresh Pool

Jérôme Vialard and Pascale Delecluse

Laboratoire d'Océanographie Dynamique et de Climatologie, Unité mixte de recherche, CNRS/ORSTOM/UPMC, Paris, France

(Manuscript received August 16, 1996, in final form August 18, 1997)

DOI: 10.1175/1520-0485(1998)028<1071:AOSFTT>2.0.CO;2

ABSTRACT

A set of numerical simulations of the tropical Pacific Ocean during the 1985–94 decade is used to investigate the effects of haline stratification on the low-frequency equilibrium of the Coupled Ocean–Atmosphere Response Experiment region. The simulated sea surface salinity structure is found to be quite sensitive to the freshwater forcing and to the other fluxes. Despite this sensitivity, several robust features are found in the model. Sensitivity experiments illustrate the important role of the haline stratification in the western Pacific. This stratification is the result of a balance between precipitations and entrainment of subsurface saltier water. It inhibits the downward penetration of turbulent kinetic energy. This results notably in a trapping of the westerly wind burst momentum in the surface layer, giving rise to strong fresh equatorial jets.

The model is able to produce a barrier layer between 5°N and 10°S in the western Pacific and under the intertropical convergence zone (as in the Ando and McPhaden composites), but also around 10°S, 120°W, where there are no data to validate its presence. The barrier layer thickness in these regions is found to be sensitive to local water forcing, and its spatial structure is governed by the large-scale circulation. The heat budget of the upper-ocean mixed layer is analyzed in these barrier-layer regions. The Lukas and Lindström hypothesis that the surface heat flux should be near zero in these regions in order to maintain the weak temperature gradient between the mixed layer and the barrier layer does not seem necessary. A significant part of the solar heat flux is lost beneath the thin mixed layer, attenuating the heating of the surface layer and allowing barrier layer maintenance in the presence of a positive net heat flux. Conversely, the development of the barrier layer is associated with a dramatic decrease of the entrainment cooling, or even entrainment heating, especially near the equator. On the whole, the barrier layer seems to insulate the SST from the effects of atmospheric forcing.

Table of Contents:

- [Introduction](#)
- [The modeling approach](#)
- [Mean simulated circulation](#)
- [Upper-layer structure](#)
- [Summary](#)
- [Discussion](#)
- [REFERENCES](#)
- [APPENDIX](#)
- [TABLES](#)
- [FIGURES](#)

Options:

- [Create Reference](#)
- [Email this Article](#)
- [Add to MyArchive](#)
- [Search AMS Glossary](#)

Search CrossRef for:

- [Articles Citing This Article](#)

Search Google Scholar for:

- [Jérôme Vialard](#)
- [Pascale Delecluse](#)

1. Introduction

Recent advances in the understanding of the El Niño–Southern Oscillation (ENSO) phenomenon suggest that air–sea interactions in the western Pacific (hereafter referred to as WP) are important in the onset of such an event ([Lukas 1988](#)). The atmospheric circulation is indeed very sensitive to the sea surface temperature in this region. The mechanisms driving the variability of temperature are thus essential in the understanding of the coupled ocean–atmosphere system response. At first glance, salinity plays a very little role in these coupled interactions. However, it has been suggested that the amount of oceanic heat directly available for the atmosphere in the upper layer of the warm pool can be dependent on the haline stratification. This is due to the so-called “barrier layer” phenomenon (hereafter referenced as BL; BLT will stand for barrier-layer thickness) ([Lukas and Lindström 1991](#)). A BL is present when the isohaline layer is shallower than the isothermal layer (see [Fig. 1](#)). In such a case, the mixed layer depth is controlled by the salinity stratification. The underlying water has a potential temperature close to the SST. A deepening of the mixed layer (e.g., under the effect of a wind burst) will not affect surface temperature via entrainment cooling. That is why the water column between the bottom of the mixed layer and the top of the thermocline has been named the barrier layer. Using data from [Levitus \(1982\)](#), the presence of the BL in the three tropical oceans has been recognized to be not just a sporadic event but a climatological feature ([Sprintall and Tomczack 1992](#)). Moreover, a strong time variability of the BL has been observed and linked to interannual variability ([Delcroix et al. 1992](#); [Sprintall and McPhaden 1994](#)).

Several questions arise from the existence of such a structure. First, is it significant enough on the surface-layer heat budget to allow the formation of large-scale SST warm anomalies? Then, what allows such a structure to appear and persist on a seasonal timescale? In order to maintain a BL, the water of the mixed layer has to remain at the same temperature as the underlying BL. Does the net surface heat flux need to be close to zero in the WP in order to maintain the weak vertical temperature gradient between the surface layer and the BL as suggested by [Lukas and Lindström \(1991\)](#)? This study tries to address these questions using OGCM simulations. This paper (Part I) investigates the role of salinity in the physics of the WP warm and fresh pool. The modeling framework and the surface forcings are presented. Of course the large-scale modeling technique has its limits and some of them might be reached in this study of the fine mixed layer processes of the WP where high frequency and small-scale processes might be important (e.g., [Tomczack 1995](#); [Chen and Rohstein 1991](#)). Much care will thus be taken in this paper to test the sensitivity of the simulated processes to the forcing and the resolution. Robust results of this study include the trapping of atmospheric fluxes in the surface layer of the warm pool by haline stratification, the role of the penetrative solar heat flux in the heat budget of the upper layers of the WP, and the impact of the BL on entrainment fluxes, especially near the equator. An associated paper (Part II, this issue) goes more deeply into the details of the large-scale BL formation processes and interannual variability.

This paper is organized as follows. [Section 2](#) describes the modeling approach. The simulated circulation and its sensitivity to the forcing and to some model parameters are described in [section 3](#). The sensitivity of the vertical mixing to the haline stratification gives some insights on the role of the salinity in the physics of the warm pool. In [section 4](#), the upper-layer structure of the warm pool is examined. A BL structure is found in the model results and its impact on the upper-layer heat budget is analyzed. [Section 5](#) summarizes the more important results of this study. The uncertainties and shadow areas that remain are then discussed in [section 6](#).

2. The modeling approach

a. The model

The model used for this study is the OPA primitive equation OGCM. It has been developed at the LODYC (Laboratoire d’Océanographie Dynamique et de Climatologie) by Delecluse’s team. The basic assumptions and the set of discretized equations using tensorial formalism are described in [Delecluse et al. \(1993\)](#). The main assumptions and parameterizations are summarized here:

- Primitive equations, including potential temperature and salinity
- Rigid lid approximation on the top
- Turbulent closure hypothesis: it is assumed that small-scale horizontal and vertical transports can be evaluated in terms of diffusion coefficients and derivatives of the large-scale flow.

The equation of state is computed from the UNESCO formulation ([Millero and Poisson 1981](#)). The equations are discretized with a second-order finite-difference scheme on an [Arakawa \(1972\)](#) C grid. The temporal scheme is a leapfrog scheme with an [Asselin \(1972\)](#) filter except for vertical diffusion, which uses an implicit scheme, and the horizontal diffusion, which uses a forward scheme.

b. Adaptation for a tropical Pacific experiment

1) PHYSICS OF THE MODEL

The LODYC model has been adapted for a medium-resolution simulation of the tropical Pacific Ocean circulation by [Maes et al. \(1997\)](#) to study the effects of the horizontal diffusion on the large-scale patterns of equatorial dynamics. The domain covers the tropical Pacific between 30°N and 30°S and between 130°E and 75°W. It has a 1° zonal resolution and a meridional resolution varying from 0.5° at the equator to 2° at the northern and southern boundaries. The vertical resolution varies from 10 m in the first 120 m to 1 km at depth (20 levels). A time step of 5400 sec (1.5 h) is used.

No-slip boundary conditions and no flux conditions for heat and salt are applied at the bottom and along the coastlines and boundaries. A damping toward the [Levitus \(1982\)](#) monthly temperature and annual salinity is used near the southern and northern boundaries in order to account for fluxes into and out of the domain. In the 20°N–20°S band, the ocean is left free.

We use a Laplacian horizontal diffusion with a constant coefficient of $10^3 \text{ m}^2 \text{ s}^{-1}$ [see [Maes et al. \(1997\)](#) for a detailed discussion of the sensitivity of the model results to the choice of this coefficient]. The vertical eddy coefficients are computed from a 1.5 turbulent closure model in which the evolution of the turbulent kinetic energy is given by a prognostic equation ([Blanke and Delecluse 1993](#)).

We want to study finescale mixed layer processes in the WP. Resolution is of primary importance for these processes. Vertical resolution is important to capture the vertical stratified (e.g., [Tomczack 1995](#)) and sheared ([McPhaden et al. 1992](#)) structure of the warm pool. Horizontal resolution should also try to capture at best the finescale horizontal structures that can appear in the warm pool. We have thus tested the sensitivity of our model results to the use of higher resolutions (see [Table 1](#) for a summary of the sensitivity experiments used in this study). The model was run with a 5-m vertical resolution from the surface to 120-m depth ([Table 1](#), experiment A7). After three years of spin up, the results of the A7 and C (control) experiments were compared for the year 1985. Differences are weak (figure not shown). Furthermore, they appear mostly in the central Pacific where A7 displays a mixing layer depth that is 10 m shallower than C in the vicinity of the equator. This is presumably due to a different representation of the shear in the transition zone between the South Equatorial Current (SEC) and the Equatorial Undercurrent (EUC). The OPA model has also been adapted by [Maes \(1996\)](#) for a high-resolution study of the three tropical oceans (with a 0.33° meridional resolution at the equator, a zonal resolution between 0.33° and 0.75°, and 30 levels). Experiment H1 of his model is similar to our control experiment in every respect except resolution. Experiments C and H1 display very similar results. Our choice of the horizontal and vertical resolution is thus a good compromise between model performance and computational cost.

2) THE FORCING

We used daily forcing issued from the Arpege Atmospheric General Circulation Model (AGCM) Atmospheric Model Intercomparison Project (AMIP) T42L30 experiment ([Déqué et al. 1994](#)). Surface fluxes of momentum, heat, and salinity are prescribed through the use of wind stress, freshwater budget, and net heat flux at the sea surface:

$$\begin{aligned}(K_m \partial_z U_h)_{z=0} &= \tau / \rho_0 \\ (K_\rho \partial_z S)_{z=0} &= (e - p) S \\ (K_\rho \partial_z T)_{z=0} &= [Q^* + \gamma(T - T^*)] / (\rho_0 C_p),\end{aligned}$$

where U_h is the horizontal projection of velocity, T the temperature, S the salinity, ρ_0 the reference density, C_p the seawater specific heat, K_m and K_ρ respectively the momentum and tracer vertical mixing coefficients, τ the wind stress, $e - p$ the freshwater budget (no runoff), and Q^* the nonpenetrative part of the surface heat flux. A penetrative solar radiation corresponding to a Jerlov type I water ([Jerlov 1968](#)) is used.

The strong coupling between surface ocean heat loss and SST is approximated by a local restoring term toward observed sea surface temperature T^* ([Reynolds 1988](#)). In a forced framework, such a restoring term is needed in order to avoid unrealistic temperatures induced by heat forcing biases. The restoring coefficient $\gamma = \partial_{\text{SST}} Q^*$ is taken equal to $-40 \text{ W m}^{-2} \text{ K}^{-1}$ everywhere. This constant value is chosen because the study made by [Oberhuber \(1988\)](#) for γ gives only slight variations around $-40 \text{ W m}^{-2} \text{ K}^{-1}$ in the Tropics [see [Dandin \(1993\)](#) for a detailed discussion of this value]. There is no restoring toward observed sea surface salinity because salinity does not affect directly the air–sea exchanges.

Starting from rest, with Levitus salinity and temperature, the model is spun up during two years with daily forcing obtained by averaging the 1984–93 Arpege forcing, and one more year with simulated wind stress and fluxes from 1984. We assume that the state obtained after this 3-yr spinup is representative for the state of the ocean at the end of 1984, and the model is integrated during the 1985–94 decade. This is the control experiment C.

The use of this AGCM forcing is, however, the source of several questions. First, how realistic are the forcings issued from this AGCM? Second, is the spatial and temporal sampling of the AGCM output fine enough to include all of the forcing structures that are important to our study? Let us examine what biases might exhibit the Arpege forcing. [Figure 2](#) displays a comparison between the 1985–94 Arpege forcings and monthly mean observed wind stresses ([Hellerman and Rosenstein 1983](#), hereafter HR), freshwater budget ([Arkin and Ardanuy 1989](#)), and net surface heat flux ([Oberhuber 1988](#)). One of the biases of Arpege is the eastward shift of the Walker circulation ascending branch. This results first in weak winds in the equatorial band where Arpege wind stresses are less than 0.05 Pa, whereas they exceed 0.07 in HR. This feature is associated with a stronger eastward penetration of the Australian monsoon into the WP. Eastward equatorial wind stresses indeed reach the date line in the Arpege annual cycle, whereas they remain west of 160°E in HR. The eastward shift of the convection zone is also associated with a negative evaporation minus precipitation budget extending more toward the central Pacific than in the dataset (the -1 mm day^{-1} isohyet reaches 170°W, whereas it is near the date line in the data). Convection is not only shifted eastward but is also weaker than in observations, leading to low precipitation over the warm pool (where net water flux is around -3 mm day^{-1} compared to the -6 mm day^{-1} value of data). This is also true in the eastern intertropical convergence zone (ITCZ), where Arpege does not exceed 5 mm day^{-1} , whereas the MSU precipitation product ([Spencer 1993](#)) suggests 11 mm day^{-1} . Arpege also has a tendency to form a “mirror ITCZ” south of the equator, which is evidenced by occasional freshwater fluxes into the ocean between 160°W and the American coast around 5°S. As in many other atmospheric models, the long-term estimate of the net heat flux into the ocean is nearly correct, but with both shortwave heat gain and latent heat losses overestimated by 40 W m^{-2} ([Dandin 1993](#)). Finally, the intraseasonal variability of Arpege surface fluxes (and especially wind stress) is underestimated ([Slingo et al. 1996](#)). The Arpege surface flux dataset thus displays some identified biases. It was chosen because it provides an interannual high-frequency (daily) coherent forcing dataset over the whole Pacific. Furthermore, forcing the model with Arpege was an introductory experiment for further coupled studies.

One might, however, wonder whether the daily forcing frequency is enough to deal with the BL processes. The BL is indeed closely linked with fine mixed layer processes. The diurnal cycle was suggested to be important in its formation. [Chen and Rohstein \(1991\)](#), for instance, included a diurnal cycle in their one-dimensional BL formation model. An experiment was conducted with an idealized shortwave heat flux diurnal cycle computed from Arpege daily forcing (see [Table 1](#), experiment A6). The introduction of this diurnal cycle had no effect at all on the simulated mixing layer and BLT. This result has, however, to be considered with care, relative to the coarse resolution of the upper-ocean layers (10 m) with respect to the diurnal cycle vertical scale. Tests conducted with a one-dimensional (and 0.5-m vertical resolution!) mixed layer model suggest an explanation to this lack of sensitivity: except just after a strong rain event, the diurnal cycle concerns mainly a layer 20 m thick situated above the top of the BL ([Josse 1996](#)). The same study, however, suggests that the occurrence of rainfall at evening or night might have a stronger effect than in the morning.

3. Mean simulated circulation


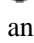
a. Large-scale structure

The general ability of the model to reproduce the large-scale major patterns of the equatorial circulation is presented in [Maes et al. \(1997\)](#). Identical main features are found when considering the mean state of our experiment (east–west thermocline tilting, deep equatorial countercurrent, etc.), although we use a high-frequency interannual forcing. We will not discuss them in this study. As we are interested in the fine thermohaline structure of the upper WP and its driving mechanisms, we have to examine closely the variables controlling its mean state and variability.

As observed by [Sprintall and McPhaden \(1994\)](#), the intensity and reversals of the SEC are crucial in driving the upper-ocean structure of the WP, as well as in the subduction mechanism proposed by [Lukas and Lindström \(1991\)](#) and [Shinoda and Lukas \(1995\)](#). [Figure 3](#) shows a comparison of mean simulated and measured velocity in the surface layer ([Reverdin et al. 1994](#)). We can see good agreement of the measured and simulated mean surface circulation, though the North Equatorial Countercurrent (NECC) appears to be slightly too weak in the model (which might be partly explained by the weak wind convergence of Arpege in the ITCZ region). The variance of the surface speed (figure not shown) is also in good agreement with data, with slightly too much variability at the equator around the date line [due to excessive eastward penetration of Arpege westerlies in this region: see [section 2b\(2\)](#)]. We can thus hope that the exchanges between the western and central Pacific will be reasonably well reproduced in the surface layer.

SSS is the key parameter for the BL. The general structure of the average annual fresh and saline water distributions are roughly reproduced by the model experiment (see [Fig. 3](#)), with freshwater in the ITCZ and South Pacific convergence

zone (SPCZ) regions and saltier water in the central equatorial Pacific and the eastern subtropical maximum. However, the simulated salinity structure exhibits important biases. The fresh pool of 33 psu water appearing west of the Costa Rican coast is too salty in the model results. The weak precipitation of Arpege there, and the lack of runoff in our model, probably explain this overestimated value. In contrast, regions under the western and central ITCZ and under the SPCZ have very low Sea Surface Salinity (SSS) (with differences up to 1 psu), compared to the annual mean produced by [Delcroix et al. \(1996\)](#). The salinity in the central Pacific is also slightly too low (with equatorial surface maximum around 35 psu instead of 35.3).

To understand what drives the SSS equilibrium, we performed an experiment that allowed us to test the sensitivity of the modeled SSS to the water flux. The model was run with the Laboratoire de Météorologie Dynamique (LMD) AGCM ([Sadourny and Laval 1984](#)) AMIP experiment freshwater flux (experiment A4) and then with all the LMD fluxes (experiment A5). The LMD water flux has a structure similar to the MSU precipitation data, with very strong evaporation compared to [Oberhuber \(1988\)](#) in the subtropics (4 mm day^{-1} instead of 1) and a convection zone shifted 2000 km to the west ([Fig. 4a](#) ). The modeled SSS reveals itself to be very sensitive to the water flux with quite different structures and variability in C and A4 ([Fig. 4b](#) ). The simulated surface currents are not changed much: the differences between C and A4 are not caused by circulation changes. Experiment A4 has better SSS values near the Costa Rican coast (due to stronger LMD precipitation in this region). Oppositely, SSS is overestimated in the subtropics due to excessive evaporation, with values up to 37.2 psu, which is 1 psu more than the observed average ([Delcroix et al. 1996](#)). In the ITCZ and SPCZ regions, the improvement of the water flux forcing does not improve the simulated SSS, suggesting that the bias toward low values has an origin other than the water flux.



Advection might also be an important term in driving the SSS structure in these regions, as suggested by Levitus (85). Experiments H1, H2, and H3 confirm this idea. They exhibit quite different SSS structures, whereas they have been produced using the same water flux. The use of different heat fluxes and wind stresses lead to significantly different circulation patterns. In experiment H3, for instance, a stronger NECC leads to a better representation of the SSS in the WP ITCZ region. The forcing associated to these simulations differs by the location of the convective center of the Walker cell. It is situated far east in experiments A5 and H3, resulting in stronger easterlies all over the equatorial band. Experiment H2 stands for an intermediate situation. The easterlies are weaker and reverse over a large portion of the WP in experiment H1. These differences lead to a variable extension of the SEC in the WP in the four experiments. The monthly surface current product of [Reverdin et al. \(1994\)](#) shows an eastward penetration of the SEC that does not cross the dateline in the equatorial band. This feature depends on the wind stress in our experiments. The eastward penetration of the SEC is too strong in experiments H3 and A5 (with westward velocities all through the equatorial Pacific), leading to a penetration of the central equatorial salty water tongue into the WP freshwater pool (hereafter we refer to the <35 psu equatorial water lying between 10°N and 10°S in the WP as the fresh pool). In contrast, the slightly overestimated reverse of the SEC in the WP of experiment H1 results in an eastward shift of this fresh pool. Here H2 stands as an intermediate. Wind forcing is also an important factor in driving the haline structure of the WP, through its impact upon the zonal extension of the SEC.

Finally, freshly biased surface salinity in our experiments might also be due to weak entrainment of subsurface saltier water in the WP. This might be due to an underestimation of high-frequency wind forcing in the AGCM wind stress dataset and to the weak diapycnal mixing in the model. The weak equatorial upwelling also may lead to an underestimated salt flux into the surface layer.

Without a damping toward observed SSS, the modeled salinity structure reveals itself to be very sensitive to the prescribed water budget. It is also sensitive to the wind forcing via the simulated circulation. Despite this sensitivity, our modeling results were robust to most changes in the surface forcing.

b. Sensitivity of the circulation to the salinity effects in the vertical mixing

We investigate in this section the impact of haline stratification on the equilibrium of the warm pool. Via its effect in the equation of state, the salinity indeed contributes to the vertical stratification, and thus to the turbulent kinetic energy dissipation. [Miller \(1976\)](#) used a one-dimensional mixed layer model to show that the inclusion of salinity could modify the surface-layer heat balance by inhibiting vertical mixing. To understand the impact of salinity stratification on the vertical fluxes in the upper layers, an experiment is conducted where the turbulent processes are solved without considering the salinity stratification. This can be done in the model by computing the potential density as a function of temperature only (salinity was fixed to 35.5 psu in the equation of state). The potential density is indeed used to evaluate the turbulent kinetic energy dissipation/production by the stratification ([Blanke and Delecluse 1993](#)). Resolution is otherwise conducted as usual, including the salinity prognostic equation. This simulation is referred to as A1.

Experiment A1 reveals several major differences with the control experiment. [Figure 5a](#)  displays the difference of the modeled mixing layer depth (defined as the layer with a vertical diffusion coefficient larger than $5 \times 10^{-4} \text{ m}^2 \text{ s}^{-1}$) between experiments C and A1. [Figure 5b](#)  displays the surface zonal current difference. In the equatorial WP, neglecting salinity effects results in a deeper mixing layer in A1. Salinity increases the vertical stratification and opposes the penetration of turbulent kinetic energy into the ocean associated with wind stirring or convective events. Both atmospheric water and

momentum fluxes are thus distributed over a thicker ocean layer in A1 experiment, which results in saltier water in the WP. The westerly wind stresses that blow west of the date line during the Australian monsoon, westerly wind bursts, or El Niño events are also distributed over a thicker layer, resulting in weaker surface jets in A1. This results in average westward currents all through the equatorial band in the A1 experiment, whereas the surface flow is on average eastward west of the date line in the control experiment (see [Fig. 5b](#)). Furthermore, the inclusion of salinity results in stronger zonal current variability (associated to eastward jets) as can be spotted from the zonal speed variance over the C and A1 experiments (figures not shown). By trapping the westerly wind stresses in the surface layer of the fresh pool, the salinity seems to have an active effect on the zonal advection, which in turn is a determinant for the warm and fresh pool displacements ([Picaut et al. 1996](#); [Delcroix and Picaut 1998](#)). The asymmetry in the haline effect on the response of the upper ocean in this region (the trapping of the westerly stresses being more effective than the trapping of easterly stresses) might be explained by nonlinear effects. The meridional convergence indeed traps zonal momentum near the equator in an eastward jet whereas the momentum diverges away from it in a westward current.

Salinity thus traps the atmospheric fluxes in the surface layer of the warm pool by controlling the mixing layer depth in this weakly thermally stratified region. The salinity stratification might actively contribute to the warm pool equilibrium by helping to set up the zonal convergence, which drives its eastern edge position ([Picaut et al. 1996](#)). It is, however, difficult to fully assess the role of salinity in the warm pool equilibrium in this forced framework, because of the damping toward the observed SST. The modeled warm pool is indeed constrained to stay close to the observed one because of this corrective surface heat flux.

4. Upper-layer structure in the western Pacific fresh pool

a. Horizontal distribution of the barrier layer

The model results have been used to map a mean BLT in the Pacific Ocean, as well as its variance (see [Figs. 6a and 6b](#)). The criterion we use to compute the BLT is the one used by [Sprintall and Tomczack \(1992\)](#). In their study, the BLT is determined by the difference between the depth of the ($SST - 0.5^\circ\text{C}$) isotherm and the depth of the $[\text{sea surface density} + \partial\rho/\partial T(SST, SSS) \cdot (-0.5^\circ\text{C})]$ isopycnal, representative of the salinity stratification accounting for the same density change as a 0.5°C temperature variation. It has been chosen because the vertical resolution of the model (10 m in the surface layers) does not allow use of the vertical gradient criterion of [Lukas and Lindström \(1991\)](#). However, both criteria give similar results with measured profiles ([Ando and McPhaden 1997](#), hereafter AM).

The mean simulated BLT over the 1985–94 period ([Fig. 6a](#)) is in good agreement with the composite for normal years of AM ([Fig. 6c](#)). The thickest BLs occur in the equatorial region, in a 10°S – 5°N latitude range between 140°E and 170°W . Two areas of thick BLT and strong BLT variability can be distinguished in this region: one at the equator and the other in the 3° – 7°S band ([Figs. 6a and 6b](#)). The root mean square of the simulated BL in both these regions is of the same order as the mean BL itself, suggesting it can sometimes totally disappear.

We will now explore the differences between our results and AM's analysis. A BL also appears in the southeastern part of the basin in our study (around 12°S , 120°W) but is missing from the AM composites. This region is, however, situated in a gap between available data points. It is thus difficult to say whether thick modeled BLs exist there. This BL formation region is not simply the result of an Arpege “mirror ITCZ.” It is indeed a robust feature of the results when using a different freshwater budget (e.g., experiment A4). The simulated BL field is systematically thinner than the measured one. In the equatorial region west of the date line, the modeled BL ranges from 10 to 15 m, whereas the AM composite ranges from 20 to 30 m. Additionally, a 10-m-thick BL extends eastward to 120°W under the ITCZ, whereas our control experiment does not display such a thick BL in this region.

Several experiments allow us to test the sensitivity of the BL to wind and heat forcing. A recent work by [Maes \(1996\)](#) suggests that the high-frequency variations (2–60 days) of wind stress are important to remove heat out of the warm pool. The H1 and H2 experiments use the same water flux (Arpege) but different heat flux and wind stress forcing [respectively Arpege and ECMWF analyses]. The Arpege wind and heat flux forcing lack high-frequency variability (compared to ECMWF analyses or data). The H2 experiment results in a deep top of the thermocline in the WP, whereas experiment H1 displayed a shallow one (compared to XBT data) ([Maes 1996](#)). This results in a thicker BL in experiment H2. The underestimation of high-frequency wind forcing partly explains the weak BLT values of our control experiment and suggests that the wind stress and the heat fluxes play a role in determining the BL depth. This is confirmed by experiment A5, involving all the LMD forcings, where the easterlies are strong all over the Pacific. BLT in the WP is indeed very weak in this simulation, whereas it is increased when using the LMD water flux only and other Arpege forcing. The sensitivity of BL processes to the prescription of the water flux is tested in experiment A4 by using the surface water flux from the LMD AGCM and the other forcing from Arpege. [Figure 7](#) displays the BL average and its variance for experiment A4. The LMD water flux (see [Fig. 4a](#)) is globally stronger (and closer to the observations) and results in thicker BLs, especially under the ITCZ. That the BL is comparable to the AM composites that appear under the ITCZ in experiment A4 and not in the C experiment suggests that direct freshwater forcing plays an important role in this region. In the warm pool and under the SPCZ, the stronger precipitation of the A4 experiment also results in thicker BLs, but to a lesser extent. This might be

another clue to the thin BLs of the control experiment in this region. A new patch of thick BLs appears south of the equator near 150°W in experiment A4. This patch is the result of a BL formation mechanism linked to meridional advection and described in Part II of this paper. Finally, the LMD water flux displays a higher frequency and smaller spatial scale structure than the Arpege field. This is reflected by the BLT in the WP, more variable in experiment A4 due to the halocline variability. Whereas the large-scale variability of the BLT seems to depend on the upper current structure (see Part 2), its small scale and high frequency variability in the WP is associated, at least partially, with the precipitation fields.

Let us also recall that the diurnal cycle had nearly no effect on the modeled BL (experiment A6). This means certainly that the large-scale process of BL formation is not influenced by the diurnal cycle. This does not exclude that other smaller scale BL formation processes not simulated here might be connected to this diurnal cycle.

We showed in [section 3a](#) that the simulated circulation and the thermohaline structure agree qualitatively with observed patterns. We noted in the previous section that the main features of this haline structure were quite robust to the use of different forcing (A4, H1, and H2 experiments). This brings us some confidence in the processes that we have analyzed in the control experiment.

b. Vertical structure of the barrier layer and associated heat transport

The simulated profiles of temperature and salinity in the WP are often very similar to those observed by [Lukas and Lindström \(1991\)](#) or displayed in AM (see [Fig. 8](#)). In such cases, the top of the thermocline is much deeper than the top of the pycnocline, which is controlled by the haline stratification. A BL is present. Two questions arise from such a structure: Is the entrainment heat flux reduced because of the weakly thermally stratified bottom of the mixed layer? Is the net heat flux over this region very weak in order to maintain the weak vertical temperature gradient between the surface mixed layer and the BL ([Lukas and Lindström 1991](#))? A mixed layer budget method (described in [appendix A](#)) allows us to compute the average temperature tendency terms over the time-varying mixed layer depth. They feature advection (in three directions), horizontal diffusion, heat forcing, and entrainment. We can answer the two previous questions by computing the average budget of the surface layer over the situations in which a thick (>10 m) BL is present in a WP box of experiment C ([Table 2](#)), this (6°S–6°N, 150°E–170°W) box is defined in a region where the BL is often thick: see [Fig. 6a](#).]

The heat advection tendency terms are weak in the WP, as well as the horizontal eddy mixing of heat (e.g., the zonal advection has values around -1.1 W m^{-2} versus 12.8 W m^{-2} in the equatorial central Pacific, vertical advection is 0.1 W m^{-2} versus -5.5 W m^{-2} in the central equatorial Pacific). Horizontal advection and eddy mixing are weak because the temperature is nearly homogeneous in the warm pool region. Temperature is also weakly stratified at the bottom of the mixed layer due to the BL: vertical advection is also very small. Only the meridional advection averaged over 6°N–6°S is significant (6 W m^{-2}), reflecting the poleward heat transport of equatorial heat by gyre systems. However, too much attention should not be given to advection terms averaged over a box including several current regimes. We are more interested in defining what vertical transfers of heat between the surface and subsurface layer (by atmospheric forcing, entrainment, and vertical advection) are typical of BL situations. Two facts are intriguing when considering this vertical heat transport. One point is that the entrainment flux and vertical advection at the bottom of the mixed layer are positive (e.g., the surface is heated up by the subsurface). This is unusual in the tropical ocean, where the cooler water is supposed to lie below the warmer. The other point is that the atmospheric forcing results in a negative tendency for the mixed layer (around -6.5 W m^{-2}), whereas the net surface heat flux is positive (around 13 W m^{-2}).

The clue to both these points appears in the vertical structure of the ocean in the presence of a BL. In many simulated BL situations, the temperature profile shows an inversion supported by salinity stratification (see [Fig. 8](#)). Such a feature is also found in the BL profile displayed in AM. In these cases, the water of the surface mixed layer is slightly cooler than the underlying BL (about 0.1°C). Oceanic data collected at the Institut Français de Recherche Scientifique pour le Développement en Coopération (ORSTOM) center of Noumea ([Delcroix and Eldin 1995](#)) has been investigated to see whether such inversions are common in the ocean. A systematic search on 1512 CTD profiles from the Comprehensive Ocean–Atmosphere Response Experiment (COARE) region (defined by the oceanic area bounded by 10°N–10°S, 140°E–180°) shows that 41% of the profiles in which a BL is present (with an average value of 27 m) display a significant temperature inversion below the mixed layer. Patches of low salinity with slightly reduced temperature have furthermore been observed in the COARE region ([Tomczack 1995](#)). This suggests that the temperature inversions in the BL are not a model bias, but an average characteristic of the stratification in the WP. The vertical scale of these inversions is about the vertical scale of the BL (27 m in data and 20 m in the model) and can certainly not be attributed to water mass intrusions that are of a smaller (1–10 m) vertical scale ([McPhaden 1985](#)). These inversions can be easily understood by considering the vertical distribution of atmospheric forcing in the WP upper ocean. The net surface heat flux over the COARE area in our control experiment is between -10 and 20 W m^{-2} (with a 13 W m^{-2} mean) over the 1985–94 period. This is in the range of climatological estimates, which give around 20 W m^{-2} into the warm pool ([Oberhuber 1988](#)). This net heat flux includes an incoming Arpege solar heat flux of about 235 W m^{-2} , which is distributed over the first 100 m of ocean ([Jerlov 1968](#); [Siegel](#)

et al. 1995) and a nonsolar heat loss. This heat loss stems mostly from latent and longwave heat fluxes at the ocean surface. It is redistributed by turbulent processes over the whole mixed layer. The resulting atmospheric forcing of the surface mixed layer is expressed in Eq. (9) of appendix A, where Q_s is the incoming solar heat flux and $Q_s f(-h)$ is the fraction of this flux leaving the mixed layer. If this fraction is larger than the net heat flux, the overall effect of atmospheric forcing is to cool the mixed layer. That is what explains the negative value of atmospheric forcing of the mixed layer in Table 2 (Table 2), whereas the net heat flux is positive. The explanation of the positive entrainment terms follows naturally. Under the average condition of heat forcing encountered in the WP, the surface layer of the model has a tendency to cool. The underlying layer is below the effects of surface mixing: it does not feel the effect of the cooling surface flux Q^* but gets some heat from penetrative solar heat flux. Under the frequent rain conditions encountered in the WP, this differential heating (described in more detail in appendix B) favors the development of temperature inversions. This situation leads to a positive entrainment of 2.5 W m^{-2} (Table 2) over the BL regions in our control experiment. It can include both eddy mixing of mixed layer water with subsurface warmer water and convective overturning when salinity stratification is not strong enough to stabilize the inversion.

Some observations and other model studies depict similar processes. Convective overturning in freshwater lenses has been monitored during the COARE Intensive Observing Period (IOP) by Tomczack (1995). Cooling of the surface mixed layer, in presence of positive net heat flux and entrainment are depicted by Anderson et al. (1996) in the same region. Schneider et al. (1996) describe a similar effect of penetrative heat flux in a CGCM (coupled general circulation model). This brings us some confidence in the model results. However, the Arpege solar heat flux is 40 W m^{-2} stronger than average annual estimates [see section 2b(2)]. This results in a slight overestimation of the differential heating in the control experiment [as can be noted from Eq. (11) of appendix B]. We have thus applied Eq. (11) to average annual heat flux data to verify that the penetrative solar heat flux might be responsible for the development of an inversion under the thin mixed layer conditions present in the WP. The average annual solar heat flux in the WP is around 195 W m^{-2} (Lewis et al. 1990). Several studies suggest that the net surface heat flux into the WP is around 20 W m^{-2} (e.g., Oberhuber 1988), Q^* thus being close to -175 W m^{-2} . Several studies using local estimates, however, suggest that this net surface heat flux is near zero, Q^* thus being close to -195 W m^{-2} (Lukas and Lindström 1991; Godfrey and Lindström 1989; Godfrey et al. 1991). We have used both these values of Q^* in our computations summarized in Fig. 9. A 40-m average mixed layer depth of the equatorial WP ocean was used (Delcroix et al. 1992; AM). The result is a $-0.15^\circ\text{C}/\text{month}$ differential cooling with climatological values and $-0.48^\circ\text{C}/\text{month}$ when following a zero surface heat flux hypothesis. In both cases, the surface fluxes have a tendency to create a temperature inversion stabilized by haline stratification. The $-0.48^\circ\text{C}/\text{month}$ value (equivalent to a 30 W m^{-2} heat flux) seems too strong to be compensated by other fluxes in the warm pool region, where advection is weak and where low winds and thin mixed layer exclude a strong vertical mixing. The zero heat flux hypothesis is thus not necessary to explain the BL upholding in the presence of a slightly positive net heat flux. The penetrative solar heat flux indeed leads to a slight cooling of the thin mixed layer and slight warming of the BL. Entrainment stemming from convective activity and wind stirring brings some heat back in the surface layer. This allows the surface layer to keep nearly the same temperature than the underlying layer.

The previous argument is based on long-term averages of the heat fluxes and mixed layer depth. These quantities have a strong variability over various timescales, including the diurnal cycle. We, however, think that our argument holds for seasonal to interannual timescales. With the previous values of Q^* ($Q^* = -175 \text{ W m}^{-2}$), we can compute the minimum net heat flux that would heat up the surface layer by 0.5°C more than the underlying layer, thus destroying the BL (see appendix B). The result is 72 W m^{-2} during one month, 57 W m^{-2} during three months, or 37 W m^{-2} during one year. The BL can thus resist long periods of positive net heat flux. Observations and 1D model results (Anderson et al. 1996) including the diurnal cycle support the role of penetrative solar heat flux in creating temperature inversions. These inversions are also present in experiment A6, suggesting that the previously described heat budget is also valid when including the diurnal cycle. Several studies, however, suggest that the mixed layer heat budget should display hysteresis in relation to the diurnal cycle. Rain events at specific hours of the day may, for instance, interact nonlinearly with mixed layer depth (Josse 1996); nighttime mixing should be active at greater depth than the halocline (Anderson et al. 1996). Only microstructure measurements and vertical heat budget sampling diurnal to interannual variability in the warm pool will provide more insight about the role of the penetrative solar heat flux in the heat budget in this region.

c. Impact of the barrier layer on the surface-layer heat budget

The previous section showed that the presence of BL could influence vertical heat transport by cutting off entrainment and vertical advection. We will now evaluate whether variability of the BL is large enough to significantly modify the surface-layer heat balance of the WP by stopping the entrainment cooling. Figure 10 displays the histogram of the entrainment as a function of the BLT, over the entire COARE region, and over a 2°N – 2°S , 170°E – 180° region. In both regions, the entrainment flux is correlated with the BLT. There is a significant difference between oceanic situations without a BL (with an average entrainment heat flux of -18 W m^{-2} in the equatorial box) and situations with a thin ($10 \text{ m} = 1$ model level) BL (with an average entrainment near zero). Further increase of the BLT is associated with an increasing positive

entrainment. This increase of positive entrainment BLT (greater than 10 m) occurs within the entire COARE box. Positive entrainment is thus a feature common to all BL situations, and not to equatorial situations only.

The values of entrainment without a BL reach -18 W m^{-2} in the equatorial region, whereas they do not exceed -5 W m^{-2} over the COARE box. This might be explained by the strong shear turbulence in the equatorial region, compared to extraequatorial latitudes. In equatorial regions, zonal acceleration is directly forced by the wind momentum penetration, which is very sensitive to the stratification. This results in a strong and variable vertical shear. The mixed layer depth displays high-frequency variations at the equator, associated with a strong variable entrainment. The entrainment flux is thus more strongly dependent on the BL absence/presence at the equator than at higher latitudes. The BLT variability near the equator should thus be studied with care.

A way to assess the role of haline stratification in the heat budget of the warm pool is to use sensitivity experiments where the salinity effects in the vertical mixing are switched off (experiment A1). Let us discuss the differences between the simulated SST of experiments C and A1. The 28°C and 29°C isotherms are shifted west by about 275 km in A1 where the warm pool is colder. This can be partly attributed to increased westward currents near the dateline (see section 3c) associated with upwelling and increased westward advection of central Pacific water ($<27^\circ\text{C}$). This can also be linked to increased entrainment in A1 in the WP. The surface flux formulation for both C and A1 experiments includes a damping toward observed SST. It is thus difficult to fully evaluate the impact of the haline stratification on the SST in these experiments. We thus conducted two supplementary experiments, in which we switched off the heat flux feedback term in the WP. In A2 and A3 experiments, γ [see section 2b(2)] is set to 0 inside the 15°S – 15°N , 140°E – 180° box and smoothly interpolated to $-40 \text{ W m}^{-2} \text{ }^\circ\text{C}^{-1}$ within 5° of the borders of this area. Experiment A3 has no salinity effects in vertical mixing computations (see Table 1). The main impact of eliminating the damping term is an increased SST variability. The model response to atmospheric forcing is stronger. For example, SST around 150°E dramatically decreases after a wind burst in February 1986 in experiments A2 and A3, whereas the feedback term kept SST near observed values in the standard case. The increased variability leads to biases with the observed values up to 1.5°C . However, the general structure of the warm pool is not affected (homogeneous temperature, longitudinal displacements, etc.). The model SST is now very different in A2 and A3. Average SST (for the year 1986 in Fig. 11) is globally colder in A3 in the western tropical Pacific (with differences up to 0.5°C near the equator at the date line). This supports the idea that the haline stratification has a braking effect over the entrainment cooling of the surface layer. This effect is stronger near the equator, as suggested above. More precisely, the colder SST in experiment A3 is the result of competition between several processes. First, the increase of entrainment cooling due to the fact that the mixed layer extends down to the top of the thermocline. Meanwhile, the surface heat fluxes are distributed over a different thickness. The deeper the mixed layer, the more it retains the penetrative solar heat flux, and the less sensitive it will be to the surface cooling. This is certainly why A3 is in some places warmer than A2. These sensitivity experiments prove qualitatively the role of haline stratification in the vertical mixing of air-sea properties into the ocean. However, they are conducted without any atmospheric feedback over the WP. Therefore they cannot help to estimate the relative importance of salinity-related processes in the onset of El Niño. The effect of the BL on entrainment might indeed be emphasized or damped by atmospheric feedbacks. A quantitative analysis of the role of salinity in the upper-ocean budget of the WP might be conducted with a coupled ocean–atmosphere model.

5. Summary

A primitive equation medium resolution model of the tropical Pacific was run over the 1985–94 decade to investigate the role of the haline structure in the physics of the warm pool. The control experiment is forced by the daily surface fluxes from the AMIP simulation of the Arpege AGCM. The only damping toward observed values in the 20°N – 20°S band is a local restoring term toward Reynolds (1988) SST in the surface heat flux. The surface salinity and circulation of this experiment are compared with available data and with sensitivity experiments using other forcing. The simulated surface circulation of the control does compare well with the observations. The westward penetration of the SEC is shown to be clearly related to the intensity and westward penetration of the easterlies. The general structure of the fresh and saline water mean distribution are reproduced by the control experiment, but several strong (up to 1 psu) biases appear. The extreme sensitivity of the simulated SSS to the freshwater forcing suggests that most of these biases could originate from its structures.

Three regions of thick (10–15 m) BL are robust in the model results. Two of them are located near the date line: one near the equator and one in the 3° – 8°S band. They correspond to regions of somewhat thicker (20–30 m) BL in AM. The last thick BLT region appears around 11°S , 120°W and cannot be validated because of the lack of data in this area. The BLT over the whole Pacific Ocean is shown to be very sensitive to the prescription of the water flux. The use of a more realistic water forcing (experiment A4) improves the BLT estimation, especially under the ITCZ where the local freshwater forcing might play an important role in the BL formation process.

The investigation of the vertical structure of the warm pool gives an insight of the vertical heat budget in this region. An inversion of the temperature profile sustained by haline stratification is often found in the BL in both model and COARE data. Following other studies (Siegel et al. 1995; Anderson et al. 1996; Schneider et al. 1996), we suggest that these inversions

might be an average characteristic of the WP, caused by the interplay of thin mixed layers and strong solar heating. In these thin mixed layer regions of the WP, a significant part of the solar heating is transmitted beneath the surface layer. Simple calculations using both model and climatological values of the surface fluxes and mixed layer depth suggest that the underlying BL might heat up at a quicker rate than the surface layer (or might heat up while the surface layer cools). This vertical distribution of the atmospheric fluxes thus lead to the growth of an inversion sustained by haline stratification. This stratification is associated to positive entrainment fluxes at the bottom of the mixed layer (mixing with deeper warmer water), which could explain how a BL can persist over long time periods in the presence of a positive net heat flux.

The impact of the BL on the surface-layer budget is then analyzed. Both sensitivity experiments and a budget method lead to the following conclusions. The haline stratification acts as a barrier against entrainment cooling of the surface layer and even switches entrainment heating on for thick BLT. The entrainment difference with or without a BL is significant enough to modify the surface-layer temperature by about 0.5°C , especially near the equator. On the opposite, thick BLs are often associated to very thin mixed layers, which retain only a reduced part of the incoming solar heat fluxes thus diminishing SST heating rate. We thus suggest that BLs should act to “uncouple” the ocean and atmosphere by inhibiting both entrainment cooling and solar heating of the surface layer. The haline stratification also inhibits downward penetration of turbulent kinetic energy in the WP ocean. This results in a trapping of westerly wind burst momentum in the surface layer of the fresh pool, giving rise to strong fresh equatorial jets. In relation with the large-scale convergence hypothesis of [Picaut et al. \(1996\)](#), we thus suggest that the salinity might have an active role in the setting of the eastern edge of the warm and fresh pool.

6. Discussion

The modeling framework and the use of AGCM daily forcing are the source of several uncertainties in this study. First, the horizontal (about 100 km) and vertical (10 m) resolution of the model might not be sufficient in comparison with the horizontal and vertical structures associated with haline effects in this region. The use of daily forcing (wiping out the diurnal cycle) can also appear insufficient. Sensitivity tests with higher resolution give very similar results, as well as tests with an idealized daily cycle. This might be partly because of the poor (275 km) resolution of atmospheric fluxes, which do not force the growth of small-scale oceanic structures. This also indicates that at least one part of BL formation and variability is related to rather large-scale and low-frequency processes. Some finescale structures ([Tomczack 1995](#); [You 1995](#)) cannot, however, be accounted for by the OGCM. These small-scale formation processes could contribute to the large-scale BL structure. Further regional modeling in the COARE region might provide more insight about these scale interactions. Moreover, a recent study has shown the impact of horizontal diffusion on the large-scale simulated circulation in the model ([Maes et al. 1997](#)). The dynamics in the warm pool is obviously dependent on parameter choices in the model and more testing about mixing is needed.

Another source of uncertainty in this study is the simulated circulation and thermohaline structure. Given the sparse time-space coverage of salinity observations, evaluation of model results is hard. There is, however, a good large-scale structure correspondence of simulated and observed SSS and BLT (AM). Several systematic biases still remain (low SSS, thin BLT), which might lead to a biased estimate of the effects of haline stratification. The simulated SSS in the WP is indeed too low. The subsurface salinity being correctly simulated, the vertical haline stratification is overestimated in the WP. This might lead to an overestimation of haline stratification effects. On the opposite, the BLT is underestimated. It is difficult to say how these opposite effects compensate.

Let us suggest some conclusions from this study.

[Cooper \(1988\)](#) already highlighted the importance of the salinity field in dynamic height computations in the tropical Pacific. We have furthermore shown the importance of haline stratification in the wind-driven dynamics of the upper layer of the fresh pool. Salinity also plays a role in the upper ocean heat budget. We strongly suggest that numerical studies of air-sea interaction covering the WP should include a salinity prognostic equation.

Our results suggest that the haline structure can significantly modify the surface layer heat budget and dynamical response. It is thus important to understand which processes govern BL formation and variability. Part II of this paper investigates the large-scale formation mechanisms in the model. It also describes their response to the interannual variability.

Finally, the “forced” framework is a strong limit in this study. To fully estimate the BL impact on the upper-ocean heat budget, the whole air-sea interaction loop has to be accounted for. We will continue the study in a coupled framework, in order to validate the effect of the BL upon the SST.

Acknowledgments

The authors thank Yves Dupenhoat, Gilles Reverdin, Roger Lukas, Mike McPhaden, and two anonymous referees for their comments on this paper. Fruitful discussions with Joel Picaut, Thierry Delcroix, and Mansour Ioualalen were appreciated. Christophe Maes developed the version of the LODYC model used in this study. Kentaro Ando and Mike

McPhaden provided very useful datasets. Gurvan Madec provided useful advice and Claire Levy useful help. Part of this work was conducted in the ORSTOM center of Nouméa. The OGCM experiments were carried on the C90s of the IDRIS center. This work was supported by the PNEDC and funded by the CNRS and the Ministère de l'Enseignement Supérieur et de la Recherche.

REFERENCES

- Anderson, S. P., R. A. Weller, and R. B. Weller, 1996: Surface buoyancy forcing and the mixed layer of the western Pacific warm pool: Observations and one-dimensional model results. *J. Climate*, **9**, 3056–3085.. [Find this article online](#)
- Ando, K., and M. J. McPhaden, 1997: Variability of surface layer hydrography in the tropical Pacific Ocean. *J. Geophys. Res.*, **102**, 23 063–23 078..
- Arakawa, A., 1972: Design of the UCLA general circulation model. Numerical simulation of weather and climate. Tech. Rep. 7, Dept. of Meteorology, University of California, Los Angeles, Los Angeles, CA, 116 pp..
- Arkin, P. A., and P. E. Ardanuy, 1989: Estimating climatic-scale precipitation from space: A review. *J. Climate*, **2**, 1229–1238.. [Find this article online](#)
- Asselin, R., 1972: Frequency filter for time integration. *Mon. Wea. Rev.*, **100**, 487–490.. [Find this article online](#)
- Blanke, B., and P. Delecluse, 1993: Variability of the tropical Atlantic Ocean simulated by a general circulation model with two different mixed layer physics. *J. Phys. Oceanogr.*, **23**, 1363–1388..
- Chen, D., and L. M. Rohstein, 1991: Modeling the surface mixed layer structure in the western equatorial Pacific (unpublished manuscript), *TOGA Notes*, **2**, 13–16..
- Cooper, N. S., 1988: The effect of salinity on tropical ocean models. *J. Phys. Oceanogr.*, **18**, 697–707..
- Dandin, P., 1993: Variabilité basse fréquence simulée dans l'Océan Pacifique tropical. Ph.D. thesis, Université Pierre et Marie Curie, 300 pp..
- Delcroix, T., and G. Eldin, 1995: Observations hydrologiques dans l'Océan Pacifique tropical ouest. TDM 141, ORSTOM, Nouméa, New Caledonia, 77 pp..
- , and J. Picaut, 1998: Zonal displacement of the western equatorial Pacific fresh pool. *J. Geophys. Res.*, in press..
- , G. Eldin, M.-H. Radenac, J. Toole, and E. Firing, 1992: Variation of the western equatorial Pacific Ocean, 1986–1988. *J. Geophys. Res.*, **97**(Suppl.), 3249–3262..
- , C. Henin, V. Porte, and P. Arkin, 1996: Precipitation and sea-surface salinity in the tropical Pacific, 1974–1989. *Deep-Sea Res.*, **43**, 1123–1141..
- Delecluse, P., G. Madec, M. Imbard, and C. Lévy, 1993: OPA version 7 General Circulation Model reference manual. Internal Rep. 93/05, LODYC, Paris, France, 140 pp..
- Déqué, M., C. Drevet, A. Braun, and D. Cariolle, 1994: The ARPEGE/IFS atmosphere model: A contribution to the French community climate modelling. *Climate Dyn.*, **10**, 249–266..
- Godfrey, J. S., and E. Lindström, 1989: On the heat budget of the equatorial west Pacific surface mixed layer. *J. Geophys. Res.*, **94**, 8007–8017..
- , M. Nunez, E. F. Bradley, P. A. Coppin, and E. J. Lindström, 1991: On the net surface heat flux into the western equatorial Pacific. *J. Geophys. Res.*, **96**(Suppl), 3391–3400..
- Hellermann, S., and M. Rosenstein, 1983: Normal monthly wind stress over the World Ocean with error estimates. *J. Phys. Oceanogr.*, **13**, 1093–1104..
- Jerlov, N. G., 1968: *Optical Oceanography*. Elsevier, 194 pp..
- Josse, P. 1996: Réponse océanique aux forçages atmosphériques dans la zone TOGA-COARE. Note de travail de l'Ecole Nationale de la Météorologie, Toulouse, France, 93 pp..
- Levitus, S., 1982: *Climatological Atlas of the World Ocean*. NOAA Prof. Paper No. 13, U.S. Govt. Printing Office, 173 pp..

Lewis, M. R., M. E. Carr, G. C. Feldman, W. Esaias, and C. McClain, 1990: Influence of penetrating solar radiation on the heat budget of the equatorial Pacific Ocean. *Nature*, **347**, 543–545..

Lukas, R., 1988: On the role of western Pacific air–sea interaction in the El Niño/Southern Oscillation phenomenon. *Proc. U.S. TOGA Western Pacific Air–Sea Interaction Workshop*, Honolulu, HI, U.S. TOGA, 43–69..

—, and E. Lindström, 1991: The mixed layer of the western equatorial Pacific Ocean. *J. Geophys. Res.*, **96**, 3343–3457..

Maes, C., 1996: Equilibre du reservoir chaud de l’Océan Pacifique tropical ouest. Ph.D. thesis, Université Pierre et Marie Curie, 255 pp..

—, G. Madec, and P. Delecluse, 1997: Sensitivity of an equatorial Pacific OGCM to the lateral diffusion. *Mon. Wea. Rev.*, **125**, 958–971.. [Find this article online](#)

McPhaden, M. J., 1985: Fine-structure variability observed in CTD measurements from the central equatorial Pacific. *J. Geophys. Res.*, **90**, 11 726–11 740..

—, F. Bahr, Y. Dupenhoat, E. Firing, S. P. Hayes, P. Niiler, P. L. Richardson, and J. M. Toole, 1992: The response of the western Pacific Ocean to westerly wind bursts during November 89 to January 90. *J. Geophys. Res.*, **97**(C9), 14 289–14 303..

Miller, J., 1976: The salinity effect in a mixed layer ocean model. *J. Phys. Oceanogr.*, **6**, 29–35..

Millero, F. S., and A. Poisson, 1981: An international one-atmosphere equation of state of sea-water. *Deep-Sea Res.*, **28A**, 625–629..

Oberhuber, J. M., 1988: An atlas based on the COADS data set: The budgets of heat, buoyancy and turbulent kinetic energy at the surface of the global ocean. Report No. 15, Max-Planck-Institut für Meteorologie, 20 pp..

Picaut, J., M. Ioulalen, T. Delcroix, M. J. McPhaden, and C. Menkes, 1996: Mechanism of the zonal displacements of the Pacific warm pool: Implications for ENSO. *Science*, **274**, 1486–1489..

Reverdin, G., C. Frankignoul, E. Kestenare, and M. J. McPhaden, 1994: Seasonal variability in the surface currents of the equatorial Pacific. *J. Geophys. Res.*, **99**, 20 323–20 344..

Reynolds, R. W., 1988: A real time global sea surface temperature analysis. *J. Climate*, **1**, 3283–3287.. [Find this article online](#)

Sadourny, R., and K. Laval, 1984: January and July performance of the LMD general circulation model. *New Perspectives in Climate Modelling*, A. Berger, Ed., Elsevier, 173–198..

Schneider, N., T. Barnett, M. Latif, and T. Stockdale, 1996: Warm pool physics in a coupled GCM. *J. Climate*, **9**, 219–239.. [Find this article online](#)

Shinoda, T., and R. Lukas, 1995: Lagrangian mixed layer modelling of the western equatorial Pacific. *J. Geophys. Res.*, **100**, 2523–2541..

Siegel, D. A., J. C. Ohlmann, L. Washburn, R. Bidigare, C. T. Nosse, E. Fields, and Y. Zhou, 1995: Solar radiation, phytoplankton pigments and the radiant heating of the equatorial Pacific warm pool. *J. Geophys. Res.*, **100**, 4885–4891..

Slingo, J. M., K. R. Sperber, J. S. Boyle, J.-P. Ceron, M. Dix, B. Dugas, W. Ebisuzaki, J. Fyfe, D. Gregory, J.-F. Gueremy, J. Hack, A. Harzallah, P. Inness, A. Kitoh, W. K.-M. Lau, B. McAvaney, R. Madden, A. Matthews, T. N. Palmer, C.-K. Park, D. Randall, and N. Renno, 1996: Intraseasonal oscillation in 15 atmospheric general circulation models: Results from an AMIP diagnostic subproject. *Climate Dyn.*, **12**, 325–357..

Spencer, R. W., 1993: Global oceanic precipitation from the MSU during 1979–91 and comparisons to other climatologies. *J. Climate*, **6**, 1301–1326.. [Find this article online](#)

Sprintall, J., and M. Tomczak, 1992: Evidence of the barrier layer in the surface layer of the Tropics. *J. Geophys. Res.*, **97**, 7305–7316..

—, and M. J. McPhaden, 1994: Surface layer variations observed in multiyear time series measurements from the western equatorial Pacific. *J. Geophys. Res.*, **99**, 963–979..

Tomczak, M., 1995: Salinity variability in the surface layer of the tropical western Pacific Ocean. *J. Geophys. Res.*, **100**, 20 499–20 515..

Vialard, J., and P. Delecluse, 1998: An OGCM study for the TOGA decade. Part II: Barrier layer formation and variability. *J. Phys. Oceanogr.*, **28**, 1089–1106..

You, Y., 1995: A rain formed barrier layer model. *Ocean Modelling* (unpublished manuscripts), **106**, 5–8..

APPENDIX A

7. Mixed Layer Heat Budget Method

As we are interested in the effect of the barrier layer presence on entrainment cooling of the surface layer, we develop a method to integrate the tracer equation over the simulated mixed layer. This method allows us to obtain the different tendency terms governing the variability of the surface temperature and salinity: horizontal advection, horizontal diffusion, forcing, and entrainment from below.

The equations of temperature are written in the model as follows (the equation for salinity being the same with different boundary condition and without the penetrative heat flux term):

$$\begin{aligned} \partial_t T = & -u\partial_x T - v\partial_y T - w\partial_z T + \partial_z(K_\rho \partial_z T) \\ & + Q_s \partial_z f(z) + D_h(T) = R, \end{aligned} \quad (\text{A1})$$

with the following surface boundary condition:

$$(K_\rho \partial_z T)_{z=0} = Q^*/\rho_0 C_p, (\text{A2})$$

where T is the potential temperature, K_ρ the vertical diffusion coefficient, D_h the horizontal diffusion operator, u the zonal current, v the meridional current, w the vertical current, $\rho_0 C_p$ the volumic specific heat of seawater, Q^* the nonpenetrative part of the surface heat flux, Q_s the penetrative solar heat flux, and $f(z)$ the fraction of solar heat flux heating that reaches the depth z , where $f(z) = R \exp(z/l_1) + (1 - R) \exp(z/l_2)$ with $R = 0.58$, $l_1 = 0.31$ m, and $l_2 = 20$ m for a Type I water ([Jerlov 1968](#)).

The mixed layer depth h , over which the tracer equation is integrated, is computed using a density criterion: the bottom of the first model level where density is higher than the sea surface density plus 0.05 kg m^{-3} . This value is chosen empirically to fit at best to the simulated mixing layer on a 1–3-day basis. (We define the model mixing layer as the layer in which the vertical mixing coefficient is higher than $5 \times 10^{-4} \text{ m}^2 \text{ s}^{-1}$. We did not use this layer to compute the surface heat/salt budget because it displays very high-frequency variations to which the tracer profiles sometimes do not have time to adjust.)

Integrating [\(A1\)](#) over the time-varying mixed layer depth, we obtain the classic integral mixed model equation:

$$\partial_t T = \frac{1}{h} \int_{-h}^0 R dz + \frac{\partial_t h}{h} (T_{-h} - \bar{T}), \quad (\text{A3})$$

where R stands for the right-hand side of (1), \bar{T} is the integrated temperature over the surface layer, and T_{-h} the temperature at the bottom of this layer.

[Equation \(A3\)](#) can be written as

$$\partial_t \bar{T} = \bar{A}_x + \bar{A}_y + \bar{A}_z + \bar{D}_h + F + E, \quad (\text{A4})$$

where

$$\bar{A}_x = -\frac{1}{h} \int_{-h}^0 u \partial_x T dz \quad (\text{A5})$$

is the zonal advection over the whole layer. (We do not separate the horizontal entrainment of interior ocean water into a sloping mixed layer by horizontal advection from the total tendency term: we found it to be negligible.) Here

is the meridional advection over the whole layer, and

$$\begin{aligned}\bar{A}_z &= -\frac{1}{h} \int_{-h}^0 w \partial_z T \, dz \\ &= \frac{1}{h} \left(w_{-h} (T_{-h} - \bar{T}) + \int_{-h}^0 (T - \bar{T}) \partial_z w \, dz \right) \quad (\text{A7})\end{aligned}$$

is the vertical advection over the whole layer; A_z is found to be nearly equal to

$$\frac{1}{h} w_{-h} (T_{-h} - \bar{T})$$

and could be included in the entrainment tendency term (10). The effect of horizontal diffusion over the layer is

$$\bar{D}_h = \frac{1}{h} \int_{-h}^0 D_h \, dz. \quad (\text{A8})$$

The combined effect of shortwave heating and surface cooling is

$$F = \frac{Q^* + Q_s [1 - f(-h)]}{\rho_0 C_P \times h}. \quad (\text{A9})$$

The overall effect of underlying water on the surface layer is

$$E = \frac{1}{h} \left(\partial_t h (T_{-h} - \bar{T}) + \frac{(K \partial_z T)_{-h}}{\rho_0 C_P} \right). \quad (\text{A10})$$

It features entrainment of water from below and turbulent flux into the surface layer.

This rearrangement of the equations is relatively easy when done using an analytical formulation. It is far more complicated with the discretized form of the equations used in OPA. This is because the [Asselin \(1972\)](#) filter mixes odd and even time steps. We have shown, using the discrete equations, that the term $e = \partial_t h (T_{-h} - \bar{T})/h$ could not be written otherwise than as the residual of the other terms from [Eq. \(A3\)](#). This implies that this term will be known to an accuracy not better than the Asselin correction term. Still, this accuracy can be increased when considering the budget over a period of several time steps. Let us say that α is the Asselin coefficient and N the number of time steps over which we compute the budget. The error made on the entrainment term is $\sim 2\alpha/N^* \partial_t T$. When the entrainment is the dominant term of the budget (i.e., $e \sim \partial_t T$, the worse case for precision), we reach an accuracy of 0.25% (we choose $N = 80$ —5 days—and α is 0.1). The second source of error in computing the entrainment as a residual from the other terms comes from the fact that the surface layer is not perfectly homogeneous in temperature or salinity. Still, this effect is negligible.

APPENDIX B

8. Atmospheric Forcing of the Mixed Layer

The net heat flux at the ocean atmosphere interface includes a penetrative solar heat flux Q_s and a nonpenetrative part Q^* that includes the sensible, latent, and longwave heat fluxes (and should also include the heat flux associated with rain events, which is not accounted for in our experiments). Here Q^* is almost always a heat loss at the ocean surface, distributed by turbulent processes over the whole mixed layer. Let us now compute the differential heat budget of the mixed layer and underlying layer, associated to the effects of surface forcing only.

For the surface mixed layer it is F as given by (A9). For a barrier thick underlying BL, the heat gain associated with forcing is due only to solar heating:

$$F' = \frac{Q_s}{\rho_0 C_p b} [f(-h) - f(-h - b)],$$

supposing that interior mixing distributes the penetrative solar heat flux over the BLT. The differential heating between the surface layer and the subsurface layer is $F - F'$. The stratification S_a (temperature difference) created by the atmospheric fluxes over a time τ between the mixed layer and the underlying layer is expressed as:

$$\frac{S_a}{\tau} = \frac{1}{\rho_0 C_p} \left(\frac{Q^*}{h} + Q_s \left(\frac{1 - f(-h)}{h} - \frac{f(-h) - f(-h - b)}{b} \right) \right). \quad (\text{B1})$$

A positive value of S_a/τ corresponds to stratification under the effect of solar heating. Using (B1), it is easy to obtain the net heat flux value necessary over a time τ to create an S_a stratification between the h meters mixed layer and the underlying layer, for a given Q^* heat flux:

$$Q_{\text{net}} = Q^* + \frac{\rho_0 C_p h \frac{S_a}{\tau} - Q^*}{1 - f(-h) - hb^{-1}(f(-h) - f(-h - b))}. \quad (\text{B2})$$

A negative value of S_a/τ results in a slower heating of the surface than of the subsurface. The temperature inversion that appears at the bottom of the mixed layer is first a source of positive *diffusive entrainment*: heating of the surface layer by eddy mixing with subsurface warmer water $[(K\partial_z T)_{-h}/(\rho_0 C_p h)]$ term of equation (A10). If this positive diffusive entrainment compensates the effects of the cooling by the atmospheric fluxes, the mixed layer remains stable. If the cooling of the mixed layer is too strong (e.g., in the case of a negative net heat flux), convective overturning starts and the mixed layer deepens until *convective entrainment* of deeper warmer water $[\partial_t h(T_{-h} - \bar{T})/h]$ term of Eq. (A10) stabilizes the mixed layer.

Tables

Table 1. Summary of sensitivity experiments used in this study.

Experiment	Resolution	Forcing fields	Vertical diffusion	Heat flux correction
C	TDH	Arpgo wind stress	(/), (S)	Yes
(Standard)	(medium resolution)	Arpgo heat flux Arpgo water flux		
A1	TDH	Same as C	(/), (S, ps)	Yes
A2	TDH	Same as C	(/), (S)	Not in WP
A3	TDH	Same as C	(/), (S, ps)	Not in WP
A4	TDH	Arpgo wind stress Arpgo heat flux LMD water flux	(/), (S)	Yes
A5	TDH	LMD wind stress LMD heat flux LMD water flux	(/), (S)	Yes
A6	TDH	Arpgo wind stress Arpgo heat flux (with thermal cycle) Arpgo water flux	(/), (S)	Yes
A7	TDH	Arpgo wind stress Arpgo heat flux Arpgo water flux	(/), (S)	Yes
(increased vertical resolution)				
H1	TOTEM	Arpgo wind stress Arpgo heat flux LMD water flux	(/), (S)	Yes
(high resolution)				
H2	TOTEM	ECMWF wind stress ECMWF heat flux Arpgo water flux	(/), (S)	Yes
H3	TOTEM	ECMWF wind stress ECMWF heat flux Arpgo water flux	(/), (S)	Yes

Click on thumbnail for full-sized image.

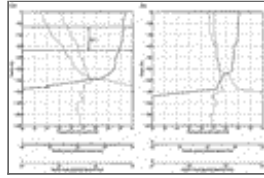
Table 2. SST tendency terms averaged over the entire COARE box during 1985–94, for all grid points where the monthly average of the barrier layer thickness is greater than 20 m (for the control experiment).

--

Zonal advection	-1.1
Meridional advection	6
Vertical advection	0.1
Horizontal diffusion	-0.2
Forcing	-6.5
Entrainment	2.5
Net surface heat flux	13

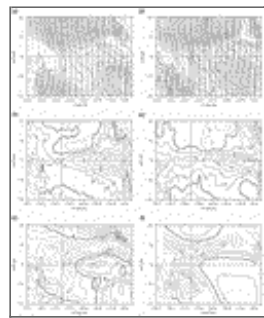
Click on thumbnail for full-sized image.

Figures



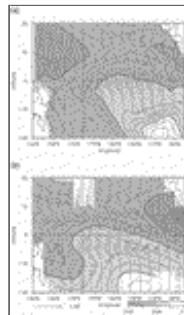
Click on thumbnail for full-sized image.

Fig. 1. Temperature, salinity, and density profiles measured during the FLUPAC campaign (a) at 177.4°W, (b) at 155.4°W. Top of the thermocline and bottom of the mixed layer computed from the (SST -0.5°C) and [sea surface density $+ \partial\rho/\partial T(\text{SST}, \text{SSS})$ (-0.5°C)] criteria are given on profile (a) where there is a thick barrier layer.



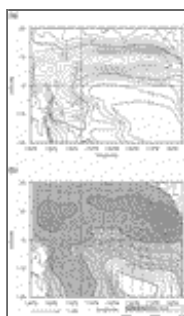
Click on thumbnail for full-sized image.

Fig. 2. Arpege forcings (a, b, c) and observed forcings (d, e, f) over the Pacific Ocean. (a) and (d) The wind stresses in N m^{-2} , with a 0.01 contour interval. (b) and (e) The net heat fluxes in W m^{-2} , with a 20 W m^{-2} contour interval. (c) and (f) The freshwater fluxes in mm day^{-1} , with a 1 mm day^{-1} contour interval. (d) From [Hellerman and Rosenstein \(1983\)](#), (e) from [Oberhuber \(1988\)](#), and (f) from [Arkin and Ardanuy \(1989\)](#).



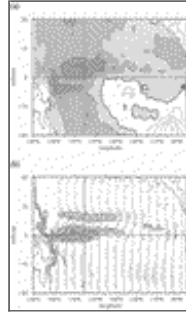
Click on thumbnail for full-sized image.

Fig. 3. Sea surface salinity and surface current (a) from our control experiment (b) from [Delcroix et al. \(1996\)](#) and [Reverdin et al. \(1994\)](#) climatologies. Contour interval for SSS is 0.25 psu.



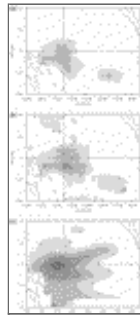
Click on thumbnail for full-sized image.

Fig. 4. (a) LMD freshwater flux averaged over 1985–94, in mm day^{-1} , with a 1 mm day^{-1} contour interval. (b) Simulated SSS (experiment A4) in psu with a 0.25 psu contour interval.



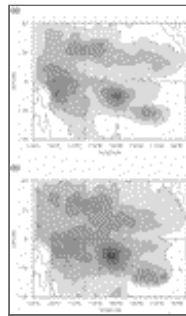
Click on thumbnail for full-sized image.

Fig. 5. The A1 experiment (without salinity in vertical mixing) minus control experiment. (a) Mixing-layer depth in meters; contour interval is 5 m , gray tones correspond to a deeper mixing layer in the A1 experiment. (b) Surface currents in meters per second, with a 5 cm s^{-1} contour interval and differences greater than 5 cm s^{-1} in gray tones.



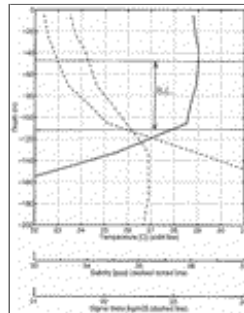
Click on thumbnail for full-sized image.

Fig. 6. (a) Simulated BLT of the control experiment (b) and its variance (from 5-day averages). (c) BLT composite for normal years from AM. Units are in meters; contour interval is 5 m .



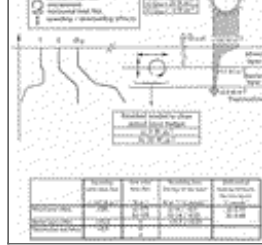
Click on thumbnail for full-sized image.

Fig. 7. (a) Simulated BLT of experiment A4 (b) and its variance (from 5-day averages). Units are in meters; contour interval is 5 m .



Click on thumbnail for full-sized image.

Fig. 8. Monthly mean temperature, salinity, and potential density simulated profiles in a situation where BL is present. Top of the pycnocline and top of the thermocline are marked by horizontal lines according to the [Sprintall and Tomczack \(1992\)](#) criterion.



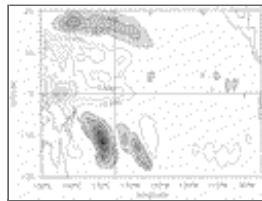
[Click on thumbnail for full-sized image.](#)

Fig. 9. Simplified vertical heat budget in presence of BL in the warm pool region. The table recapitulates the budget of the mixed layer and BL. Two hypotheses for the outgoing radiative heat flux have been selected: (a) following the climatologies and (b) following the zero net heat flux hypothesis. The fluxes arising from horizontal processes and entrainment needed to maintain a zero heating in the mixed layer are computed as the residual of the forcing terms.



[Click on thumbnail for full-sized image.](#)

Fig. 10. Histogram of entrainment flux at the bottom of the mixed layer against the 5-day averaged BLT of our control experiment. Values averaged over the COARE (10°N–10°S, 140°E–180°) box are in black. Values averaged over the 2°S–2°N, 170°E–180° box are in white. Units are in watts per square meter. The 5-day-averaged values of BLT less than 10 m mean that there was no BLT on the average, between 10 and 20 m means that there was a 1–2 model level BLT on the average, etc.



[Click on thumbnail for full-sized image.](#)

Fig. 11. SST difference between experiment A2 and experiment A3 for 1986. Units are in °C. Contour interval is 0.25 °C.

Corresponding author address: Dr. Jérôme Vialard, LODYC—Case 100, Université Pierre et Marie Curie, 4, Place Jussieu, 75252 Paris Cedex 05, France.

E-mail: jv@lodyc.jussieu.fr

[top ▲](#)



© 2008 American Meteorological Society [Privacy Policy and Disclaimer](#)
 Headquarters: 45 Beacon Street Boston, MA 02108-3693
 DC Office: 1120 G Street, NW, Suite 800 Washington DC, 20005-3826
amsinfo@ametsoc.org Phone: 617-227-2425 Fax: 617-742-8718
 Allen Press, Inc. assists in the online publication of AMS journals.